RF sputter deposition of amorphous TiO_x films: role of deposition time

A. H. Hammad [a,*] , A. Jilani [a], A. H. Milyani [b,c], G. Mousa [d], E. B. Moustafa [d], M. Sh. Abdel-Wahab [e]

[a] *Center of Nanotechnology, King Abdulaziz University, Jeddah, 21589, Saudi Arabia*

[b] *Department of Electrical and Computer Engineering, King Abdulaziz University, Jeddah 21589, Saudi Arabia*

[c] *Center of excellence in intelligent Engineering Systems (CEIES), King Abdulaziz University, Jeddah 21589, Saudi Arabia*

[d] *Department of Mechanical Engineering, Faculty of Engineering, King Abdulaziz University, Jeddah 21589, Saudi Arabia*

[e] *Materials Science and Nanotechnology Department, Faculty of Postgraduate Studies for Advanced Sciences, Beni-Suef University, Beni-Suef, 62511, Egypt*

Titanium oxide thin films were synthesized using the radio frequency (RF) sputtering technique at varying deposition times ranging from 50 to 125 min. The fabricated films display an amorphous character, with the predominant chemical state of titanium being Ti^{4+}, accompanied by a minor proportion of Ti^{3+} states. The optical absorption edges shifted to longer wavelengths, increasing from 288 to 293 nm, as the deposition time increased. The optical band gap (E_g) was indirect and decreased from 3.911 to 3.762 eV. The refractive index and dispersion parameters were evaluated and analyzed.

(Received June 30, 2025; Accepted September 4, 2025)

Keywords: Titanium oxide, RF- sputtering, Morphology, Optical transition, Dispersion properties

1. Introduction

The advancement in different technological applications is critical to the nature of the materials that compose the devices and cells. For example, the crystalline structure of titanium dioxide (*c*-TiO_2) is mainly used in photocatalytic applications, whereas the amorphous structure of *a*-TiO_2 thin films is primary used in self-cleaning surfaces, switching memory and photovoltaic applications [1–5].

In general, TiO_2 can exist in different structures, such as amorphous, anatase, rutile, and brookite [6]. However, the brookite phase can't be fabricated in its pure form [7, 8]. The amorphous phase can be prepared at low temperatures, giving significant optical transition around 3.43 eV and charge carrier dynamics, which are based on the high disorder structure and intrinsic Ti^{3+} defects [5, 9–12]. The crystalline state of TiO_2 is chemically stable and reduces the charge carrier recombination. The thermodynamic behavior of the rutile structure is more stable than the metastable anatase structure [6]. Hence, using both crystalline phases may improve the properties of photocatalytic activity and photoelectrochemical water splitting applications. In addition, *a*-TiO_2 thin layer was used to enhance the electrochromic (EC) performance and activity in the EC cell of ITO/NiO/$LiClO_4$+PC+UV gel/TiO_2/ITO [13]. Such a cell modified the induced bleached-state annihilation through preventing the β-traps during the cycling voltammetry (CV) process.

Physical and chemical routes are used to synthesize titanium oxide films, including thermal evaporation [14–16], sputtering [17–20], sol-gel processes [21–23], chemical bath deposition [24–26], and spray pyrolysis [27–30].

* Corresponding author: ahhhassan@kau.edu.sa
https://doi.org/10.15251/JOR.2025.215.513

For instance, the sol-gel process was utilized to fabricate titanium oxide (TiO_2) thin films of varying thicknesses [31]. The unheated amorphous TiO_2 was changed to the anatase phase after treated at 600 °C with a 50 nm thickness. Nevertheless, the brookite phase was observed in conjunction with the anatase phase at a film thickness exceeding 100 nm. The optical transition or the band gap of the films decreased from 3.788 to 3.687 eV as the thickness increased from 50 to 150 nm. Further, Aguilar et al. [32] have explored the photoconductivity properties of the different phases of Sol-gel TiO_2 films. The photoconductivity properties of these films were investigated under various illumination wavelengths, including 515 nm and 634 nm. The crystalline phases of TiO_2/Au films exhibited a robust photoconductivity behavior.

Grilli et al. [33] examined the properties of amorphous TiO_2 thin films that were manufactured using a radiofrequency (RF) sputtering procedure at ambient temperature in an argon (Ar) atmosphere. The researchers fabricated Schottky diodes using a nickel (Ni) contact, *n*-TiO_2, *p*-Si substrate, and an 80 nm evaporated aluminum coating for studying the junction barrier properties. The optical transition (E_g) for a thickness of 84 nm of TiO_2 thin films was estimated to 3.92 eV, while for the films with a thickness of 103 nm, the band gap was 3.84 eV. An additional investigation identified the impact of the Ar flow rate on the physical characteristics of TiO_2 thin films [34]. The improved films crystallinity was detected as the argon flow rate increased from 15 to 60 SCCM. The TiO_2 grains transitioned from sharp, needle-like shapes to dome-like shapes. The values of E_g declined from 3.65 to 3.49 eV when the rate of Ar rose from 15 to 30 SCCM. However, they remained constant at a higher flow rate, reaching 3.53 eV. For films deposited at an Ar flow rate of 15 SCCM, they exhibited a single guided mode, while all others exhibited two optical waveguide modes for transverse electric and magnetic polarizations.

The current investigation aims to delve deeply into the sputtering process that produces titanium oxide thin films at varying deposition times. The deposition time has the ability to modify the morphological and optical characteristics of TiO_x thin films, like the argon flow rate and the different film thicknesses. Therefore, the study focuses on the correlations between the deposition time and the resulting characteristics of the films, specifically their nature, morphology, roughness, chemical states, and optical and dispersion properties.

2. Experimental

On the faces of the Si wafer and glass substrate, a thin layer of TiO_2 was applied. After carefully cleaning it with a mixture of deionized water and pure ethyl alcohol, the substrate was dried with nitrogen gas. The radiofrequency sputtering method (Syskey Technologies, Hsinch County, Taiwan) was utilized in conjunction with a 99.999% pure 0.6-inch TiO_2 target. The following parameters were used in the preparation and optimization of the TiO_2 thin films: The operating pressure was 5 mTorr during the operation, and the base pressure was 9 μTorr. For the deposition of TiO_2, 200 watts of radio frequency (RF) power were applied at a temperature of 25 °C. The rate of Ar was fixed at 20 SCCM. The substrate was turnedover at 10 rpm and was spaced 14 centimeters apart. To attain different thin film thicknesses, the sputtering deposition times were 50, 75, 100, and 125 min, respectively.

The chemical states of the TiO_x thin films was completely reviewed using X-ray photoelectron spectroscopy (XPS) Versa Probe II, model XPSPHI 5000, made in USA. The spectra background was processed and corrected by the use of the Tougaard function [35, 36].

Ultima-IV Rigaku X-ray diffraction, Japan, was used to confirm the amorphous phase. A Dektak surface profiler from Burker, Germany measures the specimen thickness that was prepared at different deposition times. The measured thickness was 355, 436, 522, and 689 nm for the deposition time at 50, 75, 100, and 125 min, respectively. The Omicron UHV atomic force microscopy investigates the morphological properties of the films, while the optical spectra, including the transmittance and reflectance, were characterized via Perkin Elmer Lambda version 750, USA, from he 200 nm to 1600 nm photon wavelength range.

3. Results and discussion

3.1. X-ray diffraction

Fig. 1 demonstrates the amorphous nature of the prepared titanium oxide thin films. There are no distinct diffraction peaks in the diffraction patterns. Furthermore, the diffraction intensity values decreased as the deposition time increased from 50 min to 125 min, which could be related to the evolution of titanium oxide and resulted in a possible increase in film thickness.

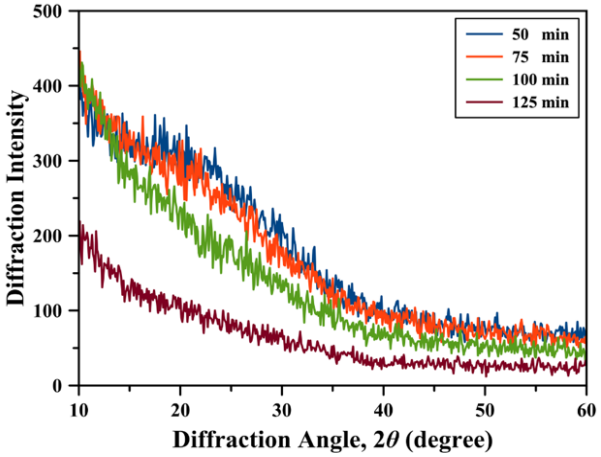

Fig. 1. The non-crystalline nature of TiO_x thin films.

3.2. The thin film chemical states

The XPS spectra of the amorphous phase of titanium oxide thin films are depicted in Fig. 2. The spectra revealed a variety of states of the elements that comprise the thin layer film, including the binding energy (B.E.) of Ti 3p at 37.6 eV, Ti 3s at 63.2 eV, C 1s at 285.6 eV, Ti 2p at 460 eV, O 1s at 530.4 eV, Ti 2s at 567.2 eV, and O KLL at 975.2 eV, respectively. Consequently, the titanium and oxygen states, as well as the contaminated carbon states [37–39], are present in the sputtered thin films that were prepared at varying deposition times. As stated in other published work, the broad presence of carbon in the environment also present in the XPS device itself led to the existence of the carbon peak [37–39].

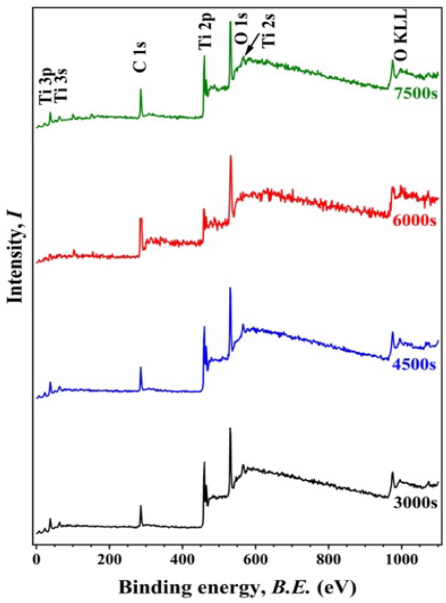

Fig. 2. TiO_x thin films spectra at different deposition times.

High-resolution of XPS is employed to conduct a more comprehensive examination of the Ti, O, and contaminated C states for each respective element for the films deposited at 125 min, as shown in Fig. 3. The other deposited films at different deposition times have the same behavior.

The HR-XPS analysis of the Ti 2p (Fig. 3a) spectrum revealed two prominent and distinct peaks at binding energy (B.E.) of 459.6 and 464.8 eV, which indicate the existence of the Ti^{4+} $2p_{3/2}$ and $2p_{1/2}$ states, respectively [1, 40–42]. Furthermore, it should be noted that there exists a minor proportion of Ti^{3+} $2p_{3/2}$ and $2p_{1/2}$ states at a B.E. of 457.8 and 466.9 eV, respectively [1, 43, 44]. The Ti^{3+} state functions as a material defect within amorphous thin films of TiO_2. The aforementioned state functions as sites for trapping charge carriers, thereby reducing electrical conduction. In addition, the observed energy difference between the $2p_{3/2}$ and $2p_{1/2}$ peaks of the Ti^{4+} state is 5.7 eV, consistent with findings reported in prior studies on TiO_2 [43, 45, 46]. Fig. 3b displays the HR-XPS analysis of the O 1s chemical state. The spectral analysis reveals the presence of two distinct deconvoluted peaks at B.E. 530.4 and 531.9 eV, corresponding to O–Ti bonds, OH bonds, and O–C bonds, respectively [1]. In addition, the carbon C 1s state is present in all thin film samples, as illustrated in Fig. 3c, as a result of the carbon's presence in the environment and the potential contamination of the thin film surface [37, 38].

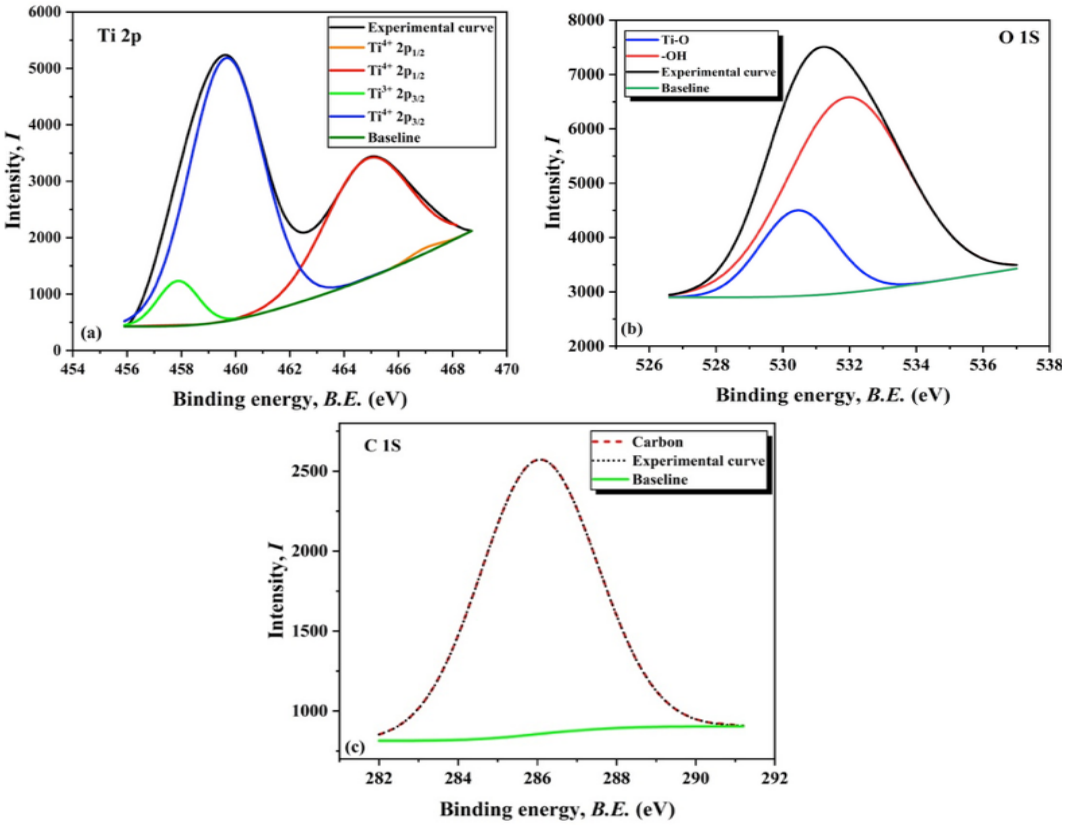

Fig. 3. The analysis of Ti 2p, O 1s, and C 1s.

Analyzing the peak area recorded in every spectrum helps one to ascertain the composition of TiO_x thin films. Table 1 shows thus the expected ratio of the TiO_x thin films, including the ratio of the carbon contamination. At a deposition time of 50 min, the carbon contamination was found to be at its lowest level (8%). As the deposition time is extended, the contamination level rises to 11.7% at 100 min.

Table 1. Thin film's elemental ratios of the TiO_x.

	The deposition time in minutes			
	50	**75**	**100**	**125**
Ti	35.8	36.2	33.2	29.6
O	56.2	54.2	55.1	61.3
C	08.0	09.6	11.7	9.5

3.3. Thin film morphology and roughness

Fig. 4 illustrates the morphology of the titanium oxide thin films in two and three dimensions. Spherical particles are observed to distribute homogeneity throughout all samples with a size or diameter measuring 26.77 nm to 30.03 nm. The particle size increased from 26.77 to 30.03 nm as the deposition time increased from 50 to 125 min. Nevertheless, the sputtered films that were deposited at 75 min exhibited the smallest size of 24 nm. Additionally, a small number of large particles can be identified in all samples. In contrast, the film's roughness is enhanced by the sputtering deposition times from 50 to 100 minutes, which decrease from 3.62 Å to 2.68 Å. The low Ti content (29.6%) of the films deposited at 125 min resulted in the highest film roughness at 4.68 Å. The particle diameter and their corresponding roughness values for various sputtering deposition times are illustrated in Table 2.

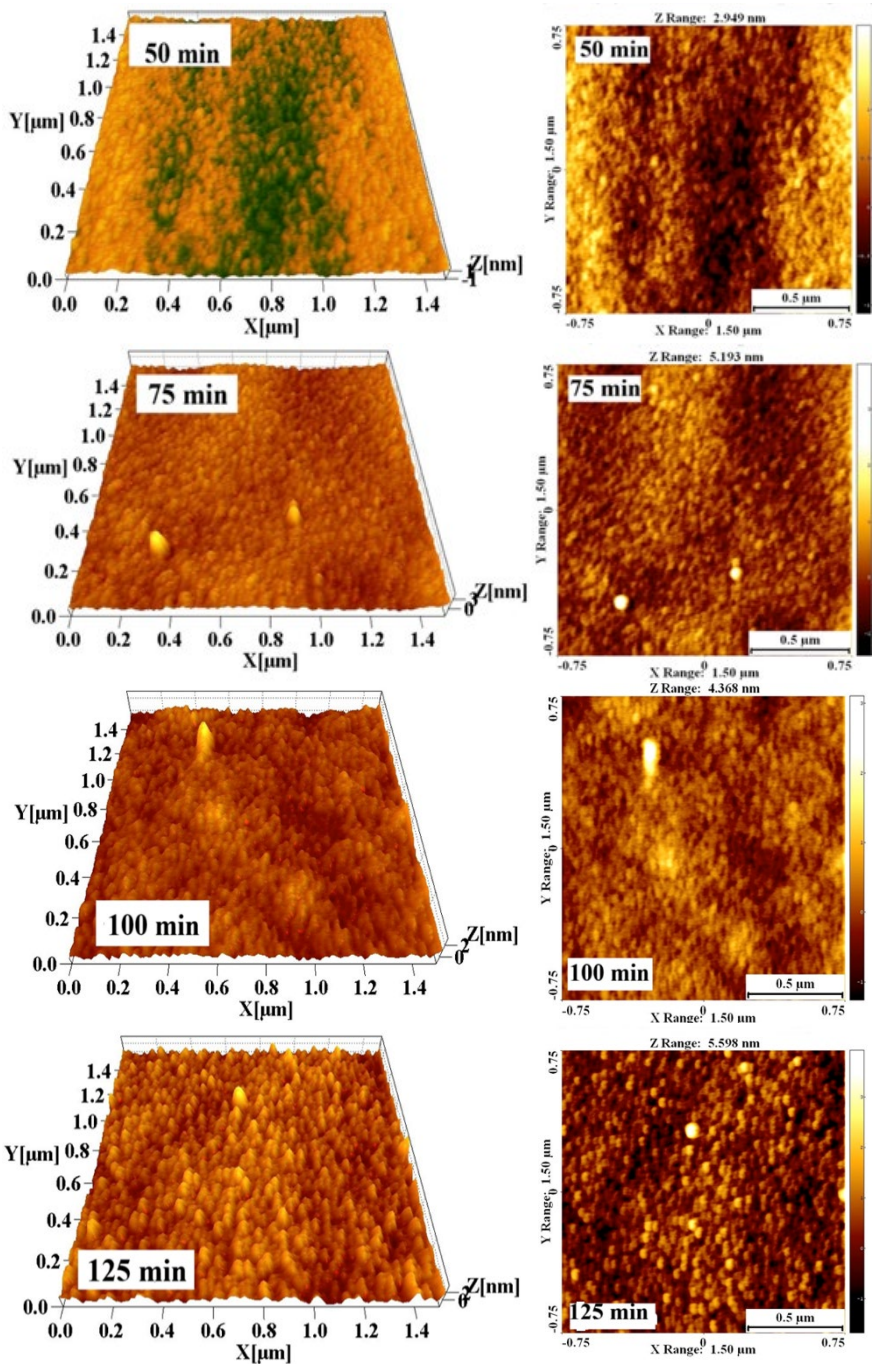

Fig. 4. The two and three dimensional film morphology and roughness images.

Table 2. Data of the particle diameter and the film roughness.

	The deposition time in minutes			
	50	**75**	**100**	**125**
Particle size (nm)	26.77	24.00	30.00	30.03
Film roughness (Å)	3.63	3.12	2.68	4.62

3.4. The optical characteristics

Fig 5 exhibited the transmittance spectra, *T*, of the TiO_x films. All the *T* spectra exhibited absorption edges, as seen in the inset figure. The absorption edge is not sharply linear due to the non-crystalline trend of the films and is shifted to higher wavelengths. For the lower deposition times at 50 min and 75 min, the *T* increased with an increase in the photon wavelength, λ to become 88.65% and 83.06% at 850 nm, respectively. At higher deposition times (100 and 125 min), the *T* decreased to 72.41% and 71.85% at λ = 850 nm. Therefore, a rise in the deposition time led to a decline in *T* values. Moreover, the films that are deposited at 100 and 125 min exhibited a better-quality optical transmittance than 50 min and 75 min as a result of the presence of a transmittance peak maximum at λ of 430 and 480 nm, respectively. Table 3 shows some optical properties of the studied films. Moreover, the optical reflectance, *R*, which is a function of the λ, was calculated from the general formula: $R(\lambda) = 1\text{-}T(\lambda)\text{-}A(\lambda)$ [47], where $A(\lambda)$ denotes to optical absorbance ($A(\lambda) = -\log(T(\lambda))$ or $T(\lambda) = 10^{-A(\lambda)}$) [47]. Fig. 5 exhibits the spectra of the optical reflectance, *R*, for different deposition times of titanium oxide thin films. Equation (1) uses the $R(\lambda)$ and $T(\lambda)$ to calculate the absorption coefficient, $\alpha(\lambda)$, as follows [48–51]:

$$\alpha(\lambda) = \frac{1}{d\ (cm)} \times ln\left[\frac{\left(1 - R(\lambda)\right)^2 + \left[\left(1 - R(\lambda)\right)^4 + 4R^2(\lambda)T^2(\lambda)\right]^{\frac{1}{2}}}{2T(\lambda)}\right] \quad (1)$$

where *d* is the thin film thickness in cm, and the extinction coefficient, $k(\lambda)$, is correlated to the $\alpha(\lambda)$ from the expression $k(\lambda) = \alpha(\lambda)/4\pi$ [52–54], as present in Fig. 6. At lower photon wavelengths in the range of 290-320 nm, the $\alpha(\lambda)$ exhibited a decrease in value from about 10^5 to 10^4 cm^{-1}, followed by a stable plateau up to 850 nm. The observed behavior is common to a number of semiconductors and can be attributed to a number of processes, such as inelastic scattering of charge carriers by phonons [55, 56].

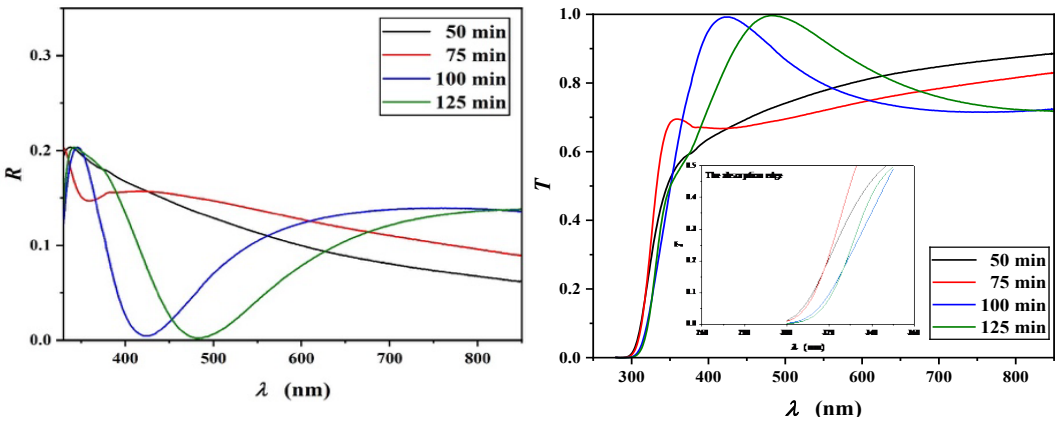

Fig. 5. The transmittance, T, and reflectance, R, spectra of TiO_x thin films.

Table 3. Some important optical parameters for titanium oxide thin films.

	The deposition time in minutes			
	50 min	**75 min**	**100 min**	**125 min**
The optical transmittance, *T* at 850 nm	0.8865	0.8306	0.7241	0.7185
The optical transmittance, *T* at 589 nm	0.7320	0.7000	0.8895	0.9950
The cut-off wavelength, $\lambda_{cut\text{-}off}$ (nm)	288	290	292	293
The optical transition (band gap), E_g (eV)	3.911	3.854	3.821	3.762
The Urbach energy, E_U (meV)	164.325	143.728	185.452	161.288

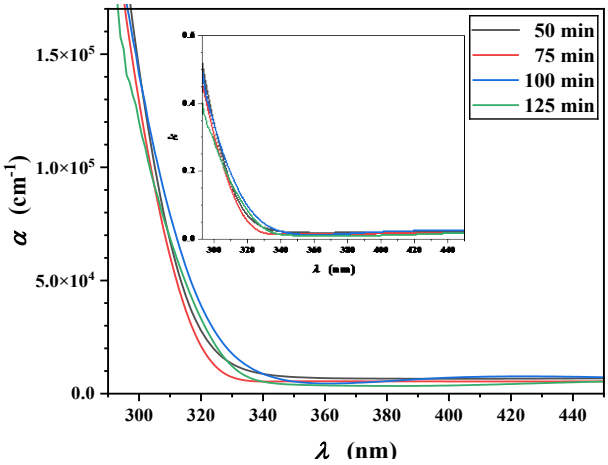

Fig. 6. The absorption edge (the inset figure), α, and, k, of the TiO_x films.

The Davis-Mott relation can calculate the optical transition, E_g, for amorphous thin films from the following equation [57]:

$$\alpha h\upsilon = constant \times \left(h\upsilon - E_g\right)^m \tag{2}$$

The optical band gap or transition is then estimated and achieved via differentiating Equation (2) [58] to become:

$$\frac{d[ln(\alpha h\upsilon)]}{d(h\upsilon)} = \frac{m}{h\upsilon - E_g} \tag{3}$$

where m denotes the optical band gap order, taking the values 2 for indirect band gap due to the amorphous nature of the films. The optical band gap is determined by plotting $d[ln(\alpha h\upsilon)]/d(h\upsilon)$ against $h\upsilon$, resulting in a peak as illustrated in Fig. 7. As the sputtering deposition increased from 50 min to 125 min, the values of E_g exhibited a decrease from 3.911 eV to 3.762 eV, as shown in Fig. 8. Therefore, this behavior is associated with the presence of the vacancy site between the bands in the Ti-O network or the defects level.

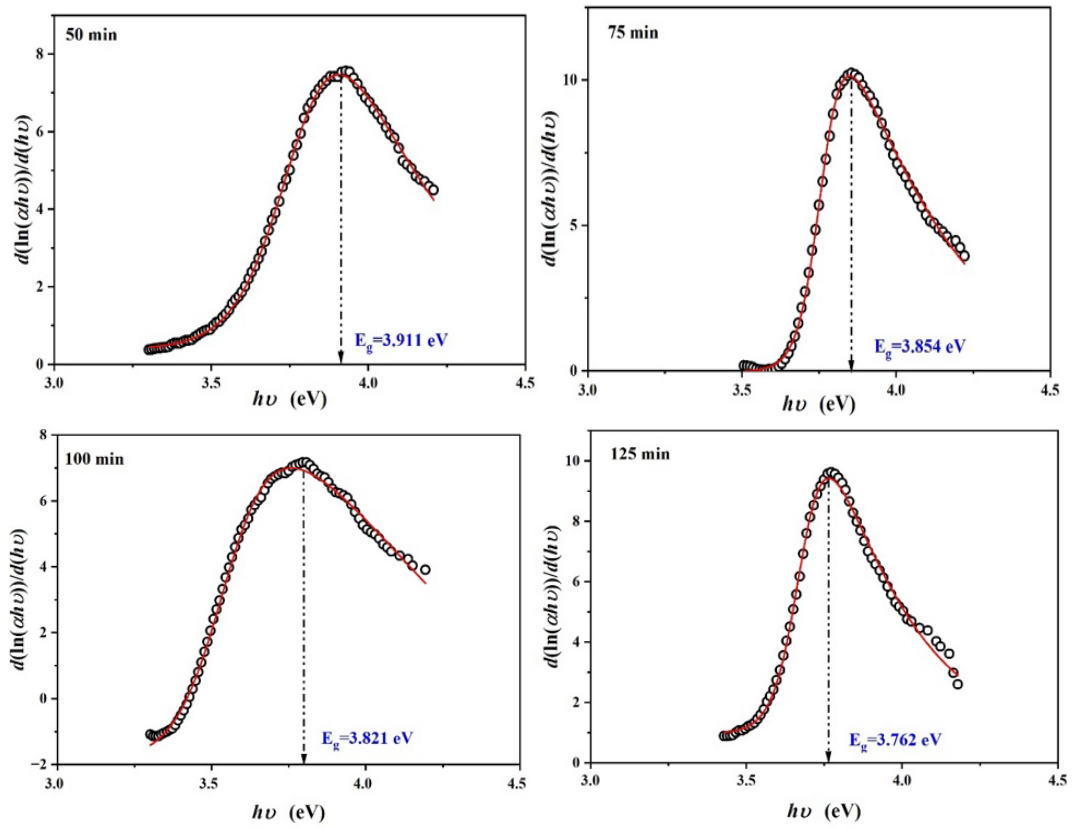

Fig. 7. Optical transition methodolgy.

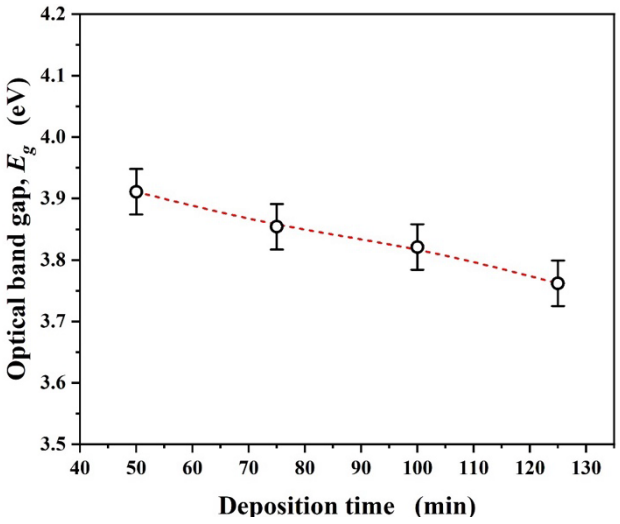

Fig. 8.The association between the energy gap (E_g) and the deposition duration.

Since the current samples are amorphous, the transition becomes indirect, meaning that m = 2. Equation (2) can be set up as follows to verify this result:

$$ln(\alpha h\upsilon) = constant + m\, ln(h\upsilon - E_g) \quad (4)$$

As seen in Fig. 9, plotting $ln(\alpha h\upsilon)$ against $ln(h\upsilon\text{-}E_g)$ results in a straight line, with the slope denoting the optical order. The indirect optical band gap in such thin films is approved when all slopes are approached to the value 2.

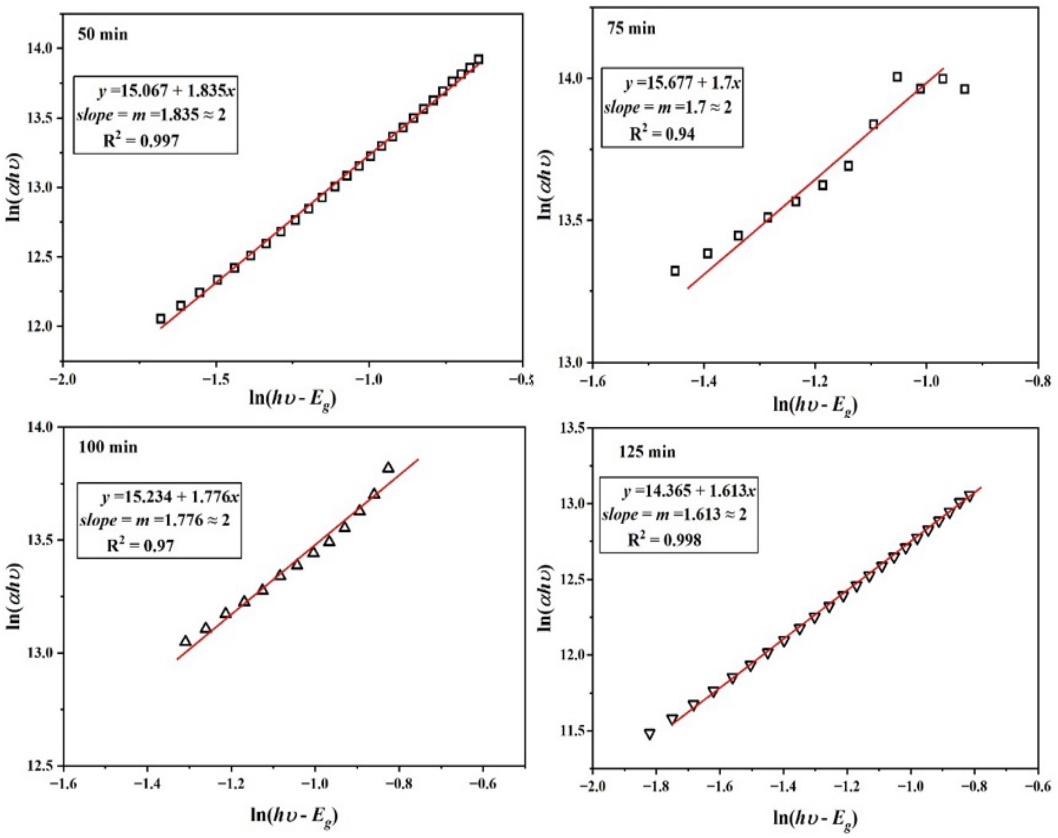

Fig. 9. The order of the optical band gap at different sputtering deposition times.

The band tail is an important characteristic in amorphous and vitreous materials, as a result of the presence of defects, vacancies, and emitting and absorbing phonons in the disordered materials. The band tail, or Urbach energy, E_U, is derived using the slope inverse of the absorption coefficient, α, logarithm, as shown in Fig. 10, which is based on the following expression [59–61]:

$$ln(\alpha) = constant + \frac{h\upsilon}{E_U} \tag{5}$$

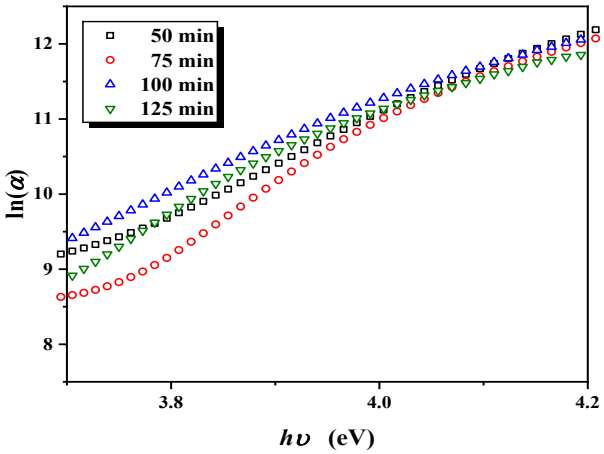

Fig. 10. The behavior of the band tail: ln(α) vs. hυ.

The Urbach energy values are shown in Table 3, which are lying in the range of 143.728 to 185.452 meV. The deposited thin film sample at 75 min exhibited the lowest E_U value at 143.728 meV, whereas the films prepared at 100 min showed the highest band tail at 185.452 meV. Therefore, the tail here in this case could depend on the titanium and oxygen content, and the defects and vacancies that could be present in the bands.

The refractive index, $n(\lambda)$ of the synthesized TiO_x films is deuced using the subsequent equation [53, 62, 63]:

$$n(\lambda) = \frac{1 + R(\lambda)}{1 - R(\lambda)} \pm \sqrt{\frac{4R(\lambda)}{\left(1 - R(\lambda)\right)^2} - k^2(\lambda)} \tag{6}$$

Fig. 11 displays how the refractive index, n, changes with different photon wavelengths in the visible and UV regions.

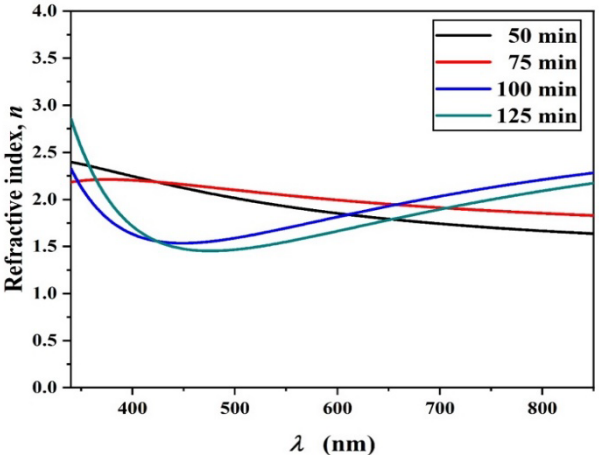

Fig. 11. The optical refractive index behavior in the UV and visible regions at different deposition times.

The single oscillator energy, E_o, and dispersion energy, E_d defines the dispersion behavior of the material, which are crucial for modulating and regulating the refractive index behavior in materials [64]. The subsequent equation delineates the relationship between the n and the dispersion parameters:

$$n^2 = 1 + \frac{E_o E_d}{E_o^2 - (h\upsilon)^2} \tag{7}$$

which may be reformulated as:

$$\frac{1}{n^2 - 1} = \frac{E_o}{E_d} - \frac{1}{E_o E_d}(h\upsilon)^2 \tag{8}$$

Consequently, a graph of the inverse of (n^2-1) against $(h\upsilon)^2$ exhibits a curve with a linear part, as illustrated in Fig. 12. The intersection of the linear line with the *y*-axis gives the value of E_o/E_d and the static refractive index, n_o $(n_o^2 - 1 = E_d/E_o)$, and the slope provides the value of $(E_o E_d)^{-1}$. Subsequently, the computed E_d and E_o are in Table 4 and Fig. 12.

Table 4. Data of the optical dispersion parameters and refractive index.

	The deposition time in minutes			
	50	**75**	**100**	**125**
The refractive index, *n*, at 589 nm	1.867	2.004	1.787	1.637
The static refractive index (n_o)	1.945	2.080	1.331	1.381
The energy of dispersion, E_d (eV)	15.505	28.168	3.102	3.530
The energy of single oscillator, E_o (eV)	5.574	8.473	4.014	3.888

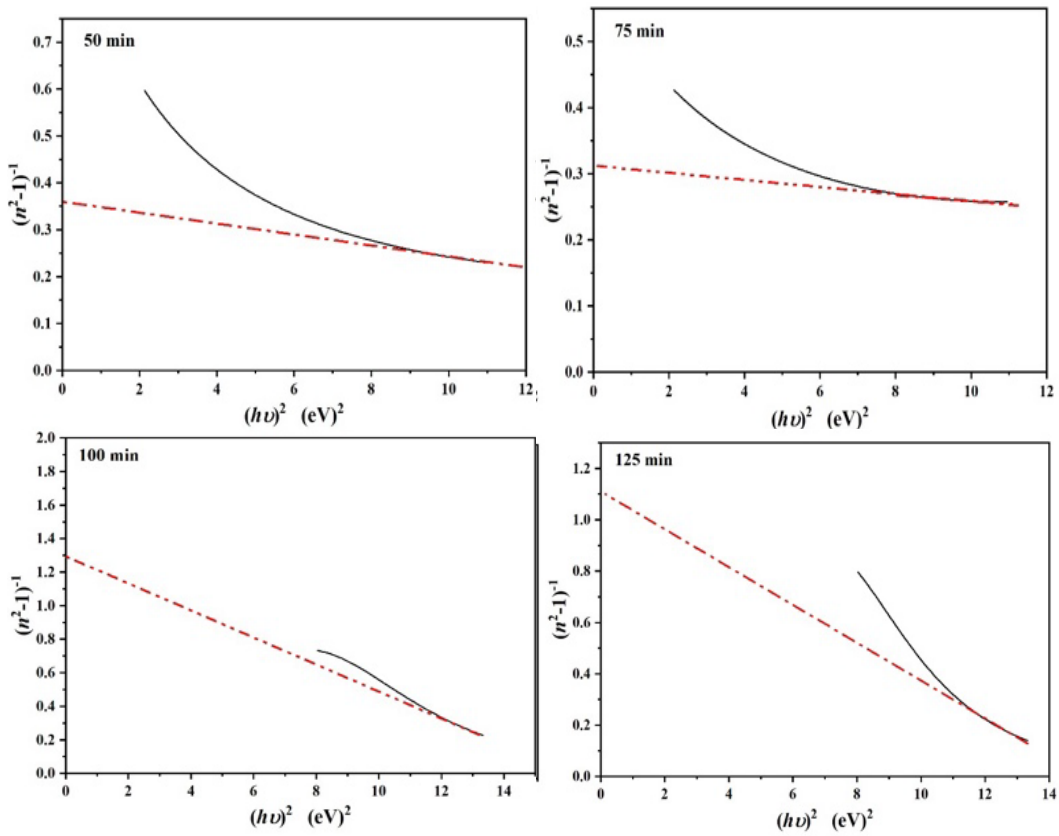

Fig. 12. Determination the dispersion parameters at different deposition times for titanium oxide thin films.

4. Conclusion

The current study investigated the titanium oxide thin films via the RF-sputtering. The sputtering deposition circle was used to control the properties of the amorphous TiO_x films. All samples exhibit an amorphous nature. The titanium states manifest as Ti^{4+} and Ti^{3+} states, each containing an excess of oxygen. All samples exhibit a homogeneous distribution of spherical particles, resulting in a decrease in roughness from 3.63 to 2.68 Å and an increase in deposition time from 50 to 100 min. The films prepared at 75 min had the smallest particle size, approximately 24 nm. At higher deposition times (100 min and 125 min), the prepared films demonstrated high optical transmittance. As the time of deposition increased from 50 to 125 min, the indirect transition (E_g) values decreased slightly, from 3.911 to 3.762 eV, which could be contributed the increase of the vacancy sites in the titanium oxide network. Depending on the deposition time, the refractive index ranged from 1.867 to 1.637 at 589 nm. This variation can tune the optical behavior of the materials under study.

Acknowledgements

This project was funded by the Deanship of Scientific Research (DSR) at King Abdulaziz University, Jeddah, under grant no. (GPIP: 615-903-2024). The authors, therefore, acknowledge with thanks DSR for technical and financial support.

References

[1] R. Mauchauffé, S. Kang, S.Y. Moon, Surf Coat Technol 376, 84(2019); https://doi.org/10.1016/j.surfcoat.2018.01.088

[2] H. Sabbah, Materials Express 3, 171(2013); https://doi.org/10.1166/mex.2013.1106

[3] H.Y. Jeong, J.Y. Lee, S.Y. Choi, Adv Funct Mater 20, 3912(2010); https://doi.org/10.1002/adfm.201001254

[4] Z. Ren, J. Wang, Z. Pan, K. Zhao, H. Zhang, Y. Li, Y. Zhao, I. Mora-Sero, J. Bisquert, X. Zhong, Chemistry of Materials 27, 8398(2015); https://doi.org/10.1021/acs.chemmater.5b03864

[5] J. Wang, Y. Shang, Appl Phys Lett 102 (14), 143113 (2013); https://doi.org/10.1063/1.4801755

[6] J. Saari, H. Ali-Löytty, K. Lahtonen, M. Hannula, L. Palmolahti, A. Tukiainen, M. Valden, J Phys Chem C 126 (36), 15357(2022); https://doi.org/10.1021/acs.jpcc.2c04905

[7] A. Di Paola, M. Bellardita, L. Palmisano, Catalysts 3 (1), 36(2013); https://doi.org/10.3390/catal3010036

[8] D. Dambournet, I. Belharouak, K. Amine, Chemistry of Materials 22 (3), 1173(2010); https://doi.org/10.1021/cm902613h

[9] B. Astinchap, K.G. Laelabadi, J Phys Chem Solids 129, 217(2019); https://doi.org/10.1016/j.jpcs.2019.01.012

[10] D. Miao, H. Hu, A. Li, S. Jiang, S. Shang, Ceram Int 41 (7), 9177(2015); https://doi.org/10.1016/j.ceramint.2015.03.080

[11] V.A. Glezakou, R. Rousseau, Nature Mater. 17, 856(2018); https://doi.org/10.1038/s41563-018-0150-1

[12] P. Nunez, M.H. Richter, B.D. Piercy, C.W. Roske, M. Cabán-Acevedo, M.D. Losego, S.J. Konezny, D.J. Fermin, S. Hu, B.S. Brunschwig, N.S. Lewis, J Phys Chem C 123 (33), 20116(2019); https://doi.org/10.1021/acs.jpcc.9b04434

[13] P. Shao, S. Huang, B. Li, Q. Huang, Y. Zhang, R.T. Wen, Mater Today Phys 30, 100958 (2023); https://doi.org/10.1016/j.mtphys.2022.100958

[14] R.S. Dariani, E. Easy, Optik 126 (22), 3407(2015); https://doi.org/10.1016/j.ijleo.2015.07.139

[15] H.I. Elsaeedy, A. Qasem, H.A. Yakout, M. Mahmoud, J Alloys Compd 867, 169150(2021); https://doi.org/10.1016/j.jallcom.2021.159150

[16] S.M. Alghamdi, H. Albalawi, S.A. Ahmad Jafri, A. Ashfaq, H. Alqurashi, E.A. Shokralla, O.A. Algethami, O.A. Albeydani, E. Alsubhe, M.M. Saad H.-E., Vacuum 222, 113013 (2024); https://doi.org/10.1016/j.vacuum.2024.113013

[17] A. El Mesoudy, D. Machon, A. Ruediger, A. Jaouad, F. Alibart, S. Ecoffey, D. Drouin, Thin Solid Films 769, 139737 (2023); https://doi.org/10.1016/j.tsf.2023.139737

[18] S. Yadav, A. Chahar, S. Singh, I. Singh, B. Birajdar, Mater Today Proc (2023). https://doi.org/10.1016/j.matpr.2023.03.404

[19] D. Stock, N. Weinberger, F. Ruske, L. Haug, M. Harnisch, R. Lackner, Thin Solid Films 786, 140115(2023); https://doi.org/10.1016/j.tsf.2023.140115

[20] A. Grayeli, A. Ahmadpourian, S. Jurečka, C. Luna, S. Rezaee, M. Karimi, Opt Mater 157, 116363(2024); https://doi.org/10.1016/j.optmat.2024.116363

[21] Z.Y. Acar, M. Asiltürk, J Nanoparticle Research 24, 162 (2022); https://doi.org/10.1007/s11051-022-05543-y

[22] S.G. Ullattil, P. Periyat, Environment and Electronic Applications (Springer, Switzerland, 2017), pp. 271; https://doi.org/10.1007/978-3-319-50144-4_9

[23] O. Jongprateep, R. Puranasamriddhi, J. Palomas, Ceram Int 41, S169(2015); https://doi.org/10.1016/J.CERAMINT.2015.03.193 https://doi.org/10.1016/j.ceramint.2015.03.193

[24] L. Zhou, R.C. Hoffmann, Z. Zhao, J. Bill, F. Aldinger, Thin Solid Films 516 (21), 7661 (2008); https://doi.org/10.1016/j.tsf.2008.02.042

[25] A.H. Mayabadi, V.S. Waman, M.M. Kamble, S.S. Ghosh, B.B. Gabhale, S.R. Rondiya, A. V. Rokade, S.S. Khadtare, V.G. Sathe, H.M. Pathan, S.W. Gosavi, S.R. Jadkar, J Phys Chem Solids 75 (2), 182(2014); https://doi.org/10.1016/j.jpcs.2013.09.008

[26] P. Manurung, Y. Putri, W. Simanjuntak, I.M. Low, Ceram Int 39 (1), 255(2013); https://doi.org/10.1016/j.ceramint.2012.06.019

[27] H. Enayati-Taloobaghi, H. Eshghi, Mater Res Bull 167, 112416 (2023); https://doi.org/10.1016/j.materresbull.2023.112416

[28] H. Attouche, S. Rahmane, S. Hettal, N. Kouidri, Optik 203, 163985 (2020); https://doi.org/10.1016/j.ijleo.2019.163985

[29] K.S. Shamala, M. Vishwas, Mater Today Proc 52, 1344(2022); https://doi.org/10.1016/j.matpr.2021.11.071

[30] T. Chandra Paul, J. Podder, L. Paik, Results in Optics 8, 100235 (2022); https://doi.org/10.1016/j.rio.2022.100235

[31] A. Taherniya, D. Raoufi, Mater Res Express 6, 016417 (2018); https://doi.org/10.1088/2053-1591/aae4d0

[32] G. Valverde-Aguilar, J.A. García-Macedo, V. Rentería-Tapia, M. Aguilar-Franco, Appl Phys A 103, 659(2011); https://doi.org/10.1007/s00339-010-6199-6

[33] M.L. Grilli, M. Yilmaz, S. Aydogan, B.B. Cirak, Ceram Int 44 (10), 11582(2018); https://doi.org/10.1016/j.ceramint.2018.03.222

[34] H. Serrar, F.Z. Mecibah, I. Kribes, Y. Bouachiba, A. Mammeri, A. Bouabellou, M. Retima, A. Boughelout, A. Taabouche, R. Aouati, Opt Mater 135, 113259 (2023); https://doi.org/10.1016/j.optmat.2022.113259

[35] I.N. Demchenko, Y. Melikhov, Y. Syryanyy, I. Zaytseva, P. Konstantynov, M. Chernyshova, J Electron Spectros Relat Phenomena 224, 17(2018); https://doi.org/10.1016/j.elspec.2017.09.009

[36] M.S. Abdel-wahab, A.H. Hammad, A. Jilani, A. Alshahrie, A.A. Melaibari, Opt Quantum Electron 53, 1(2021); https://doi.org/10.1007/s11082-021-03039-y

[37] N. Wang, X. Li, Y. Wang, Y. Hou, X. Zou, G. Chen, Mater Lett 62 (21-22), 3691(2008); https://doi.org/10.1016/j.matlet.2008.04.052

[38] T. Giannakopoulou, N. Todorova, M. Giannouri, J. Yu, C. Trapalis, Catal Today 230, 174(2014); https://doi.org/10.1016/j.cattod.2013.10.003

[39] M.S. Abdel-wahab, A. Jilani, A. Alshahrie, A.H. Hammad, J Mater Sci Mater Electron 29, 3056(2018); https://doi.org/10.1007/s10854-017-8237-z

[40] J.E. Jeong, C.Y. Lee, Thin Solid Films 788, 140178 (2024); https://doi.org/10.1016/j.tsf.2023.140178

[41] Q. Chen, Q. Liu, J. Hubert, W. Huang, K. Baert, G. Wallaert, H. Terryn, M.P. Delplancke-Ogletree, F. Reniers, Surf Coat Technol 310, 173(2017); https://doi.org/10.1016/j.surfcoat.2016.12.077

[42] C.D. Wagner, W.M. Riggs, L.E. Davis, J.F. Moulder, Handbook of X-Ray Photoelectron Spectroscopy (Perkin- Elmer Cooperation & Physcial Electronics Division, USA, 1979).

[43] B. Bharti, S. Kumar, H.N. Lee, R. Kumar, Sci Rep 6, 32355 (2016); https://doi.org/10.1038/srep32355

[44] C.H. Kim, B.H. Kim, K.S. Yang, Carbon 50 (7), 2472(2012); https://doi.org/10.1016/j.carbon.2012.01.069

[45] S.C. Ray, D.K. Mishra, A.B. Panda, H.T. Wang, S. Bhattacharya, W.F. Pong, J Phys Chem C 126 (20), 8947(2022); https://doi.org/10.1021/acs.jpcc.2c02311

[46] K. Baba, S. Bulou, P. Choquet, N.D. Boscher, ACS Appl Mater Interfaces 9 (15), 13733(2017); https://doi.org/10.1021/acsami.7b01398

[47] M.M. Damoom, A.M. Alhawsawi, E. Banoqitah, E.B. Moustafa, O.E. Sallam, A.H. Hammad, Opt Quantum Electron 56, 976 (2024); https://doi.org/10.1007/s11082-024-06909-3

[48] A.M. El-Mahalawy, A.R. Wassel, Mater Sci Semicond Process 116, 105124 (2020); https://doi.org/10.1016/j.mssp.2020.105124

[49] E.R. Shaaban, N. Afify, A. El-Taher, J Alloys Compd 482 (1-2), 400(2009); https://doi.org/10.1016/j.jallcom.2009.04.033

[50] A.M. Salem, Y.A. El-Gendy, G.B. Sakr, W.Z. Soliman, J Phys D Appl Phys 41 (2), 025311 (2008); https://doi.org/10.1088/0022-3727/41/2/025311

[51] A.R. Ansari, A.H. Hammad, M.S. Abdel-wahab, M. Shariq, M. Imran, Opt Quantum Electron 52, 1(2020); https://doi.org/10.1007/s11082-020-02535-x

[52] A.M. Salem, M.E. El-Ghazzawi, Semicond Sci Technol 19, 236 (2004); https://doi.org/10.1088/0268-1242/19/2/019

[53] A.R. Ansari, U.A. Rajput, M. Imran, M. Shariq, M.S. Abdel-wahab, A.H. Hammad, Braz J Phys 51, 499(2021); https://doi.org/10.1007/s13538-021-00891-x

[54] A.R. Wassel, I.M. El Radaf, Appl Phys A 126, 177 (2020); https://doi.org/10.1007/s00339-020-3353-7

[55] T.S. Moss, G.J. Burrell, B. Ellis, Semiconductor Opto-Electronics, 1st ed. (Butterworth-Heinemann, London, 1973); https://doi.org/10.1016/B978-0-408-70326-0.50005-3

[56] H.M. Hosni, S.A. Fayek, S.M. El-Sayed, M. Roushdy, M.A. Soliman, Vacuum 81 (1), 54 (2006); https://doi.org/10.1016/j.vacuum.2006.02.014

[57] E.A. Davis, N.F. Mott, Philosophical Magazine 22, 0903(1970); https://doi.org/10.1080/14786437008221061

[58] F. Yakuphanoglu, M. Arslan, Physica B 393 (1-2), 304(2007); https://doi.org/10.1016/j.physb.2007.01.017

[59] Z.A. Talib, W.M. Daud, E.Z.M. Tarmizi, H.A.A. Sidek, W.M.M. Yunus, J Phys Chem Solids 69 (8), 1969(2008); https://doi.org/10.1016/j.jpcs.2008.02.005

[60] A.H. Hammad, A.R. Wassel, G.O. Rabie, S.Y. Marzouk, Opt Laser Technol 161, 109134 (2023); https://doi.org/10.1016/j.optlastec.2023.109134

[61] A.H. Hammad, M.A. Marzouk, H.A. ElBatal, Silicon 8, 123(2016); https://doi.org/10.1007/s12633-015-9283-x

[62] L. Boudaoud, N. Benramdane, R. Desfeux, B. Khelifa, C. Mathieu, Catal Today 113 (3-4), 230(2006); https://doi.org/10.1016/j.cattod.2005.11.072

[63] M.M. Gomaa, G.R. Yazdi, S. Schmidt, M. Boshta, V. Khranovskyy, F. Eriksson, B.S. Farag, M.B.S. Osman, R. Yakimova, Mater Sci Semicond Process 64, 32(2017); https://doi.org/10.1016/j.mssp.2017.03.009

[64] S.H. Wemple, M. DiDomenico, Phys Rev B 3, 1338(1971); https://doi.org/10.1103/PhysRevB.3.1338